










Article

From Academia to Industry: Criteria for Upscaling Ionic Liquid-Based Thermo-Electrochemical Cells for Large-Scale Applications

Arianna Tiozzo ^{1,2}, Andrea Bertinetti ^{3,*}, Alessio Tommasi ^{3,*}, Giovanna Nicol ¹, Riccardo Rocca ¹, Sawako Nakamae ⁴, Blanca E. Torres Bautista ⁴, Sabrina Campagna Zignani ⁵, Edith Laux ⁶, Sebastien Fantini ⁷ and Mauro Francesco Sgroi ^{2,5}

¹ South Europe—Sustainable Raw Materials, Centro Ricerche FIAT S.C.p.A., Strada Torino 50, 10043 Orbassano, Italy

² Department of Chemistry, University of Turin, Via Pietro Giuria 7, 10125 Torino, Italy

³ Gemmate Technologies srl, Via Reano 31, 10090 Buttigliera Alta, Italy

⁴ Service de Physique de L'état Condensé, SPEC, CEA, CNRS, Université Paris-Saclay, CEA Saclay, 91191 Gif sur Yvette, France

⁵ Institute of Advanced Energy Technologies (ITAE), Italian National Research Council (CNR), Via Salita S. Lucia Sopra Contesse 5, 98126 Messina, Italy

⁶ Haute Ecole Arc Ingénierie (HES-SO), Eplatures-Grise 17, 2300 La Chaux-de-Fonds, Switzerland

⁷ Solvionic, 11 Chemin des Silos, 31100 Toulouse, France

* Correspondence: andrea.bertinetti@gemmate-technologies.com (A.B.); alessio.tommasi@gemmate-technologies.com (A.T.)



Citation: Tiozzo, A.; Bertinetti, A.; Tommasi, A.; Nicol, G.; Rocca, R.; Nakamae, S.; Torres Bautista, B.E.; Campagna Zignani, S.; Laux, E.; Fantini, S.; et al. From Academia to Industry: Criteria for Upscaling Ionic Liquid-Based Thermo-Electrochemical Cells for Large-Scale Applications. *Energies* **2024**, *17*, 1. <https://doi.org/10.3390/en17010001>

Academic Editors: Said Bentouba, Peter Breuhaus, Mahmoud Bourouis and Nadjet Zioui

Received: 17 November 2023

Revised: 11 December 2023

Accepted: 17 December 2023

Published: 19 December 2023



Copyright: © 2023 by the authors. Licensee MDPI, Basel, Switzerland. This article is an open access article distributed under the terms and conditions of the Creative Commons Attribution (CC BY) license (<https://creativecommons.org/licenses/by/4.0/>).

Abstract: Thermo-electrochemical cells (or thermocells) represent a promising technology to convert waste heat energy into electrical energy, generating power with minimal material consumption and a limited carbon footprint. Recently, the adoption of ionic liquids has pushed both the operational temperature range and the power output of thermocells. This research discusses the design challenges and the key performance limitations that need to be addressed to deploy the thermocells in real-world applications. For this purpose, a unique up-scaled design of a thermocell is proposed, in which the materials are selected according to the techno-economic standpoint. Specifically, the electrolyte is composed of EMI-TFSI ionic liquid supplemented by $[\text{Co}(\text{ppy})]^{3+/2+}$ redox couples characterized by a positive Seebeck coefficient (1.5 mV/K), while the electrodes consist of carbon-based materials characterized by a high surface area. Such electrodes, adopted to increase the rate of the electrode reactions, lead to a thermoelectric performance one order of magnitude greater than the Pt electrode-based counterpart. However, the practical applications of thermocells are still limited by the low power density and low voltage that can be generated.

Keywords: thermo-electricity; thermoelectric generator; thermo-electrochemical cell; ionic liquid; scale-up

1. Introduction

The growing recognition of climate change and the need to reduce greenhouse gas emissions have fueled clean energy investments in recent years at local, national, and global scales (see, e.g., the recent adoption of the EU's Green Deal Industrial Plan) [1]. A successful exit from fossil fuel dependency toward carbon-neutral and energy-self-sufficient societies requires substantial efficiency improvements in today's renewable energy technology and diversification of energy sources. Ambient and waste heat are one of the most ubiquitous renewable energies and secondary or residual energy that can be harnessed for energy efficiency improvement. Indeed, 70% of consumed primary energy is said to be 'wasted' as heat [2,3] from electronic devices (integrated circuits, phones, computers, etc.), running vehicles, in-door buildings, etc. [4]. Various waste-heat recovery technologies

exist depending on the size and temperature range of the waste heat, the organic Rankin cycles and district heating from larger industrial waste streams [5,6], and thermoelectric generators (TEGs) for smaller and mobile sources. For the latter, the transportation industry is arguably the most attractive sector for the use of TEGs [7], in particular the automotive sector, where competition towards ever-cleaner cars is very dynamic and encouraged by governments. About 70% of fuel energy is lost as waste heat in automobiles via engine exhaust and coolant [8]. Automotive fuel efficiency can be increased by the conversion of waste heat into electricity. With the transition to electric vehicles, TEGs also need to transfer their implementation from conventional vehicles to hybrid and full electric vehicles, where thermal management involves the cooling of batteries, power electronic systems, and the motor [9].

Thermoelectric (TE) materials (mostly made of inorganic semiconductors) are capable of converting heat into electricity (the Seebeck effect) and have been used to recover low-grade waste heat since the 1950s. However, its market growth has stagnated for decades due to the low efficiency of TE modules. With a recent advancement in nano-structuration technology and the development of new materials, remarkable improvements in the thermal-to-electric energy conversion efficiency (ZT) have been achieved, although their efficiency and size remain far below those of other heat engines (e.g., geothermal, Rankine cycles, etc.). Other techno-economic hurdles include the high cost of nanomaterial manufacturing, the difficulty of maintaining uniform material properties, and the use of scarce and/or toxic raw elements (Bi, Te, Se, Sb, etc.), preventing their mass deployment in high-impact market sectors, including buildings and construction (solar panels, smart windows, etc.), data centers (cooling systems), and transport (e.g., internal combustion engines and hybrid vehicles), to name a few.

Recently, unconventional TE materials such as organic polymers and gels, nanostructured carbon materials, and complex liquids (electrolytes with dissolved ions) [10] have emerged as alternative solutions to overcome the bespoke barriers. Despite their low electrical conductivity and low operational temperature range, their resource efficiency (requiring abundant and non-critical elements and facile and low-cost synthesis methods) and high shape-versatility make these new TE materials attractive, especially for low-power/low-temperature TE devices with complex shapes. Furthermore, liquids have the advantage of ensuring uniform and stable thermoelectric performance across a large material volume, making them a credible candidate for large-scale applications.

To convert heat into electricity, the thermoelectric liquids are used in a so-called thermo-electrochemical cell, or thermocell. In its simplest form, a thermocell is a thermally insulating container filled with an electrolyte with dissolved redox couple salts. Two sides of the thermocell are sealed hermetically with conducting electrodes, across which a temperature gradient (heating and cooling) is applied. The dominant phenomena for the generation of electric potential and current are the thermogalvanic and Ludwig–Soret effects.

The thermogalvanic effect describes the temperature-dependent oxidation and reduction potentials of dissolved redox species when they react with the electrodes (see Equation (1)).



The oxidant A (and reductant B) give to (and take from) n -electrons the electrodes to generate an electrical current from the thermocell. The temperature dependence of the redox reaction potential creates a voltage difference (ΔV) across the thermocell, which is related to the reaction entropy difference, ΔS_{rc} .

$$S_e = -\frac{\Delta V}{\Delta T} = -\frac{\Delta S_{rc}}{e} \quad (2)$$

ΔS_{rc} is composed of the redox-specific standard reaction entropy and Nernst's term [11,12]. The thermoelectric voltage can be further boosted by the Ludwig–Soret effect when the liquid

mixtures contain multiple types (size and charge signs) of molecules and particles. As each particle/molecule responds differently to a temperature gradient, an additional electric potential difference can be generated [13].

Despite the difference in the physical/chemical origins of the voltage creation between solid thermoelectric materials and liquid thermogalvanic systems, it has become customary to use the term Seebeck coefficient (S_e) for describing the voltage-to-temperature ratio as indicated in Equation (2). The most widely studied liquid-based thermoelectric generator was based on the $\text{Fe}(\text{CN})_6^{3-/4-}$ (ferro/ferricyanide) redox salts dissolved in water and was first reported in 1986 [11]. Ferro/ferricyanide and many other redox couple combinations exhibit S_e coefficient values above 1 mV/K, an order of magnitude larger than their semiconductor counterparts. However, the presence of water limited the use of thermocells to below 100 °C. The latest advancements in ionic liquids (ILs) with fusion points below 100 °C and boiling points above 200 °C and in nanostructured electrodes are pushing both the operational temperature range and the power output from liquid TEGs [12,14]. It should be noted that while the fundamental mechanisms of ΔS_{rc} production can be, to a good extent, described by the Born model and its phenomenological extensions [15] in weak electrolytes, the theoretical foundation of the phenomena in strong electrolytes such as ionic liquids is still lacking [16].

Several examples of small, laboratory-scale prototypes based on TE liquids are reported, reaching 12 W/m² at $\Delta T \sim 80$ °C with water mixed with $\text{Fe}(\text{CN})_6^{3-/4-}$ redox salts in a thermocell equipped with nanostructured electrodes [14,17,18]. In thermocells based on ionic liquids/solvent mixtures, a power output of ~ 0.8 W/m² was reported with $\text{Co}^{3+/2+}$ redox salts and ΔT of ~ 70 K, with a corresponding S_e value around 2 mV/K [12].

The biggest challenges in increasing the efficiency of IL-based thermoelectric generators are the solubility of redox salts and the high viscosity (at low temperatures and protonic ILs), together with the low rates of electrode reactions that hamper thermocells' power output. To boost the power output, one of the most promising solutions is the structuration of the electrodes to increase the specific surface area [19–21]. In early research, platinum group metals (PGMs), such as platinum and rhodium electrodes, were used because their high catalytic activity minimized charge transfer [12]. However, the prohibitively high cost of platinum has necessitated the development of more commercially viable electrode materials. In this regard, carbon-based electrodes are becoming increasingly important as a promising and affordable alternative to platinum electrodes. Nanostructured carbon materials, such as single (SWNT) and multiwalled carbon nanotubes (MWNT) and graphene, have a large surface area, which helps in increasing the number of reaction sites [12,22].

From a techno-economic standpoint, given the abundance of raw materials found in liquid thermoelectric systems combined with their relatively low electric conductivity and operational temperature range (compared to, e.g., Bi_2Te_3 -alloy semiconductors) [23–25], their use becomes most attractive in large-size/low-power thermoelectric generation devices.

The mission of this research is to pave the way for the adoption of thermo-electrochemical energy harvesting systems based on ionic liquids in large-scale applications. To assess the scalability of laboratory-scale thermocells, an up-scaled design conceived to fulfill the requirements of industrialization is here reported. A unique up-scaled prototype of a thermocell containing EMI-TFSI ionic liquid supplemented by $\text{Co}^{3+/2+}$ redox couples was assembled. To enhance the effective surface area of electrodes without introducing expensive solutions, cost-effective carbon-based materials were tested in combination with inert and low-surface-area coated materials to evaluate their effect on electrical power extraction.

2. Experimental

2.1. Design of the Thermoelectric Cell

The upscaled thermoelectric cell was conceived following the cold-over-hot orientation condition (see Figure 1a), which promotes natural convection and significantly increases the performance of the system thanks to the improved mass transport [12]. The cell is characterized by a sandwich-like structure where the body of the cell is placed between

the two electrodes, while Al-alloy hot and cold plates close the stack and manage the heat exchange. PEEK was selected as the material for the body of the cell since it is chemically inert and capable of operating at temperatures up to 250 °C. The cell body was designed as a network of parallel, long, thin channels to be filled with the electrolyte (see Figure 1b). The filling of the channels was managed by a common fill port when the cell was completely assembled. The filling was performed by means of a peristaltic pump connected to the fill port in a closed loop. Such a strategy makes the process cleaner and safer and allows for the electrolyte to be cycled to eliminate the air bubbles being created in the channels.

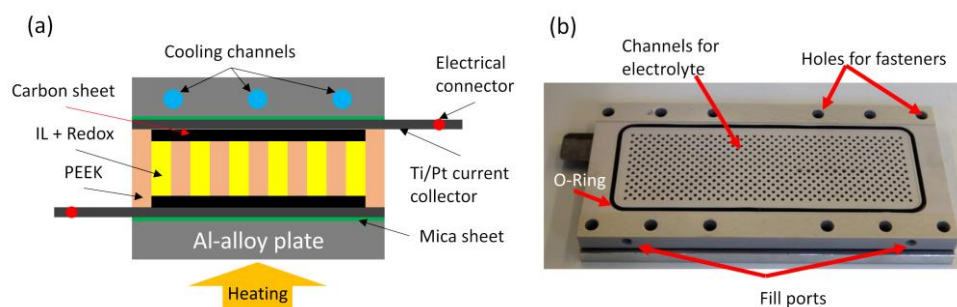


Figure 1. Thermoelectric cell used for the tests. (a) cross-section and (b) detail of the cell body.

Platinized titanium sheet (Ti/Pt) was selected as the current collector thanks to its conductivity, corrosion resistance, and cost effectiveness. Such a solution consists of a titanium sheet 1 mm thick coated with platinum (0.5 mm) on both sides. The tailored process endows the coating of a relatively high roughness that contributes to enhancing the electrode surface area. However, the process ensures that any potential exposed Ti area is oxidized to give chemical resistance to the substrate. This is a safety-first approach, as the process used for the coating ensures that the whole of the substrate is covered. Two carbon-based sheets were placed in contact between the PEEK cell body and the electrodes to enhance the electrode's effective surface area. For electrical insulation purposes, a 0.2 mm thick sheet of mica was placed between the Ti/Pt electrodes and the two external aluminum alloy plates. The 12 mm thick cold plate was designed with a set of embedded cooling channels connected to a closed-loop water cooling circuit.

2.2. Materials Selection

A wide range of ionic liquids with a wide electrochemical stability window (ESW), good ionic conductivity (σ), a wide thermal range for the existence of the liquid phase, and the ability to dissolve redox couples were thoroughly screened. In this study, 1-Ethyl-3-methylimidazolium bis(trifluoromethylsulfonyl)imide (EMI-TFSI) was finally selected as the best compromise between the properties. Among the many room-temperature ionic liquids that are commercially available today, EMI-TFSI presents the best combination of favorable thermo-electrochemical features. As such, EMI-TFSI is one of the most widely used ILs in electrochemical applications such as supercapacitors and batteries [26–28]. Responding to a high demand, EMI-TFSI is being produced in large quantities at an industrial scale, giving further advantage from the techno-economic point of view. The main physical–chemical properties of EMI-TFSI are reported in Table 1.

Table 1. Relevant properties of the EMI-TFSI ionic liquid.

ESW	σ @ 25 °C	T_{melting}	$T_{\text{crystallization}}$	$T_{\text{decomposition}}$
4.6 V	9.4 mS/cm	23 °C	−41 °C	>300 °C [29]

Among the various commercially available redox couples examined, cobalt complexes with pyridine chelating ligands (e.g., bpy (tris(2,2-bipyridine)) and ppy (tris(2-(1H-pyrazol-1-yl)pyridine)) give the highest Seebeck coefficient and power output, as well as

prolonged temperature and chemical stability [30,31]. Between the two Co redox couples, $[\text{Co}(\text{ppy})]^{3+/2+}$ was chosen for the present study for its higher availability (and thus less costly). Therefore, the ionic liquid-based electrolyte used in the prototype is composed of EMI-TFSI with a concentration of 30 mM of $[\text{Co}(\text{ppy})]^{3+/2+}$ redox couple. The diffusion coefficient was measured by following the procedure reported in the Supplementary Materials. The diffusion coefficient of the considered electrolyte was $1.7 \times 10^{-7} \text{ cm}^2/\text{s}$ at ambient temperature and $2.7 \times 10^{-7} \text{ cm}^2/\text{s}$ at 120°C .

It is well known that the surface properties of the electrode material can influence the electrochemical interface between the electrode and the electrolyte in the cell, so that the current density generated by the device can depend on the effectiveness of the discharge process of the redox couple at the electrodes. In this view, carbon-based electrodes are considered a promising solution since they are characterized by a high surface area, which increases the number of reaction sites. The four carbon-based materials considered in this research were selected because they represent a cost-effective solution already existing on the market and are largely used in other electrochemical systems such as fuel cells, where the maximization of the surface area and catalytic activity of the electrodes is of fundamental importance to obtaining high-output electric power. The first electrode material is a woven carbon cloth (hereinafter CC) purchased on FuelCellStore. In addition, two different types of carbon papers produced by SGL Carbon were considered: (i) Sigracet[®] 39AA (hereinafter 39AA), a non-woven plain carbon paper fully graphitized that has no PTFE treatment, and (ii) Sigracet[®] 39BB (hereinafter 39BB), which is characterized by a bilayer structure consisting of a macro-porous backing material (carbon fiber paper support that integrates a 5% wt of PTFE) and a microporous carbon-based layer (MPL), which contains 20 to 25 wt% PTFE. The fourth electrode consists of Sigracet[®] 39BB modified with a 15 μm thick coating that contains a fluorinate binder and a high surface area Vulcan XC-72 carbon black (hereinafter 39BB + V).

The SEM analysis was performed on the carbon materials to observe the surface morphology at high magnification. CC is a woven material made of carbon fibers with a diameter between 7.5 and 11.5 μm (Figure 2a,b). The 39AA material shows a random network of straight carbon fibers with diameters between 6 mm and 8 mm (see Figure 2c,d). The spaces between the fibers are filled by flakes-type carbon particles, which also cover the fibers. These particles derive from the manufacturing process, where the raw paper is impregnated with a carbonizable resin with the addition of carbon fillers before being cured and graphitized. Moreover, 39AA and the macro-porous backing material of 39BB (Figure 2e,f) are characterized by a similar morphology since they are produced with the same process. However, the 5% wt amount of PTFE in 39BB is clearly visible at higher magnification. On the other side, the MPL appears compact but is largely characterized by deep fractures (Figure 2g,h). The coated side of 39BB + V is shown in Figure 2i,l where the Vulcan-based coating surface appears similar to the MPL, but it is thicker because the Vulcan coating was superimposed on the microporous layer.

The composition of the materials impregnated with the IL-based electrolyte was characterized by X-ray photoelectron spectroscopy (XPS). Figure 3 illustrates the electronic states of elements exposed to the surface of carbon-based electrode materials. According to Figure 3, there are no significant differences in the elements identified on the surfaces of the four spent specimens investigated. The XPS spectra show mainly the presence of graphitic carbon, fluorine, oxide, nitrogen, and sulfur. The latter two varieties come from the interaction with the ionic liquid; in fact, they reflect the binding energy associated, respectively, with organics containing nitrogen at around 400.4 eV [32] and sulfur compounds at around 167.2 eV [33,34]. F1s has a dominant peak at 687.2 eV associated with halogenated compounds [35] related to the ionomer used for electrode preparation, which contains fluorine. However, the impregnation with EMITFSI also contributes to determining the fluorine peaks.

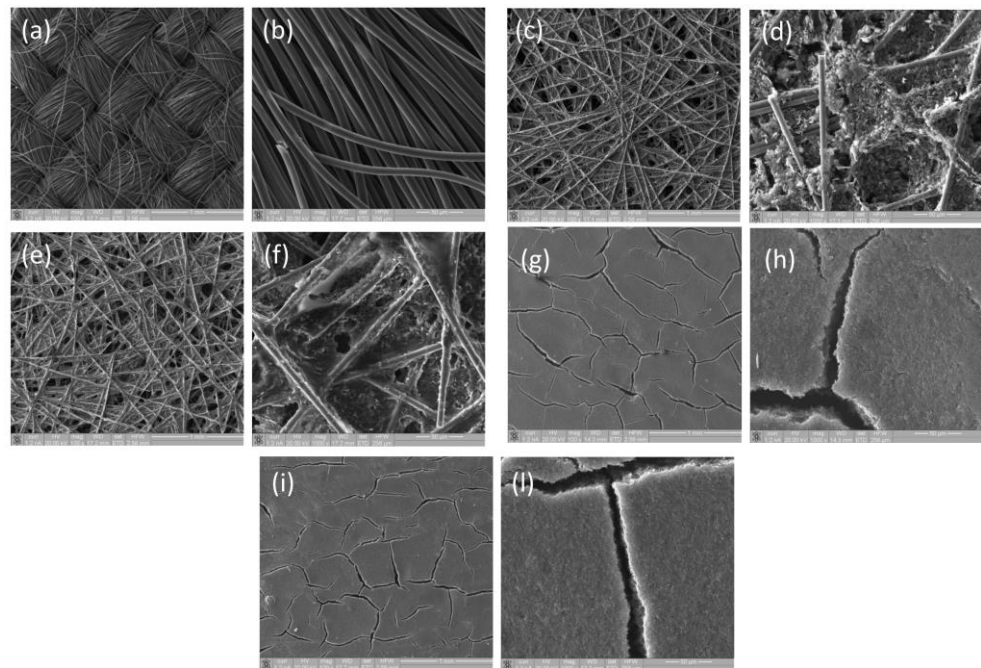


Figure 2. SEM images of carbon-based supports at 100 \times and 1000 \times magnification. (a,b) CC, (c,d) 39AA, (e,f) 39BB macro-porous backing material, (g,h) 39 BB MPL, and (i,l) coated side of 39BB + V.

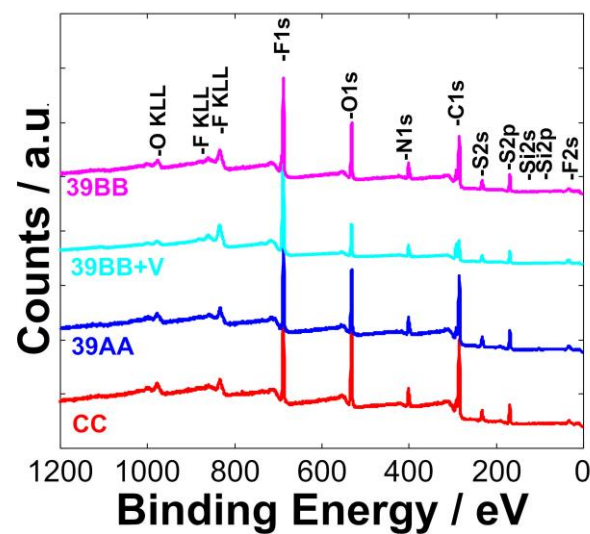


Figure 3. Results of X-ray photoelectron spectroscopy measurements performed on the carbon-based materials used as electrodes in the thermogalvanic cells.

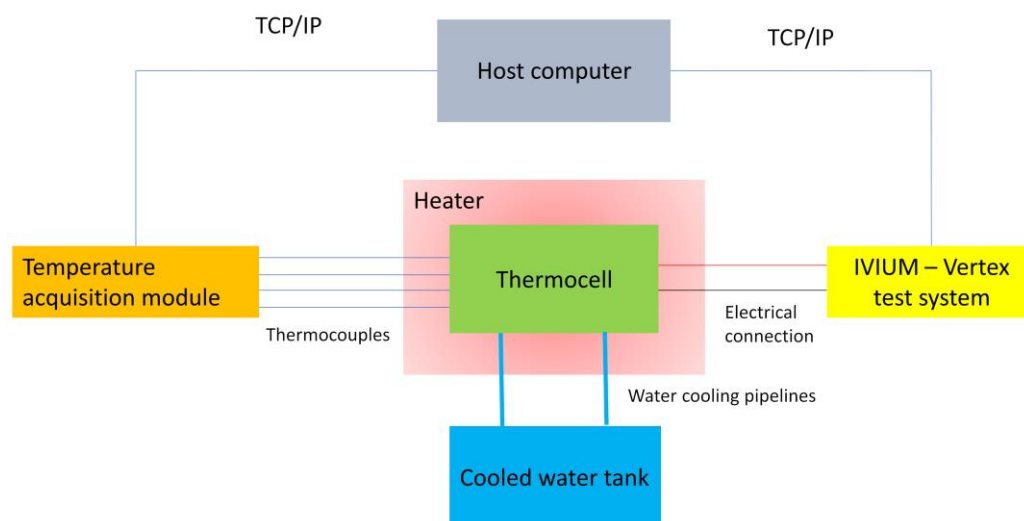
The carbon-based materials were also characterized in terms of their electrochemical surface area (ECSA) and electric resistivity. ECSA measurements were performed following the procedure detailed in the Supplementary Materials. The electric resistivity of electrode materials is measured by the determination of the V-I curve. To do that, for each material, a disk with a diameter of 6 mm is placed in a cell composed of two gold-coated electrodes to reduce contact resistance, and its thickness was evaluated using a micrometer. The electrical resistance of the sample was measured using a linear potential ramp from 0 V to 0.5 V, and the current was recorded accordingly. The resistance was calculated using Ohm's law and corrected considering the contact resistance of the measuring setup. Table 2 summarizes the characteristics of the materials considered in the present study.

Table 2. ECSA and electrical resistivity of the carbon-based materials used as electrodes in the thermo-galvanic cell.

Material	MPL	Thickness (μm)	ECSA @ $T_{\text{amb}}/T = 120\text{ }^{\circ}\text{C}$ ($1/\text{cm}^2$)	Electrical Resistivity ($\text{m}\Omega\cdot\text{m}$)
CC	No	330	3.03/2.71	49
39AA	No	280	2.71/1.47	5
39BB	Yes	315	5.46/3.41	3
39BB + V	Yes	330	4.33/3.04	46

2.3. Thermoelectric Test Setup

The thermoelectric test bench is depicted in Figure 4. The upscaled thermoelectric cell was placed on an electric heater plate in a cold-over-hot orientation. The temperature of the cell was monitored and recorded by two pairs of thermocouples, one on the hot plate and the other on the cold plate. To vary the temperature on the hot plate, the power of the heater was modulated, while the temperature on the cold plate was modified by changing the temperature of the cooling water. The average value of the temperature difference between the hot and cold plates (ΔT) is measured during each test. A series of tests was performed to fix the external condition of the cell when the temperature of the hot and cold plates stabilized after changing the operating conditions. The electrical measurements are performed from the two current collectors of the cell, one on the hot side and the other on the cold side, which are connected to a potentiostat/galvanostat test system, IVIUM—Vertex, controlled via the IviumSoft© software release 4.1098.

**Figure 4.** Setup for thermoelectric testing.

The tests on the prototype were performed at constant current (galvanostatic conditions) by changing the current every 10 s from 0 mA to the maximum value, which reduces the voltage of the cell to zero (see Figure 5a). The voltage of the cell was measured at the end of each 10 s step, which is defined as a reasonable time to obtain a stable value without extending too much the duration to reduce as much as possible temperature variation on the cell plates during the test. The measurements of the voltage and the current were used to evaluate the open circuit voltage (OCV) and the maximum power (P_{max}) at different temperatures and materials. The power is computed by multiplying the current and the voltage, and the P_{max} is obtained by evaluating the maximum of the curve obtained from each test (see Figure 5b). Apart from the testing carried out considering the different carbon materials, the cell performance was also evaluated with the Pt coating as the sole electrode. This cell, identified as “void”, was then used as a benchmark to assess the boosting introduced by high-surface-area electrodes.

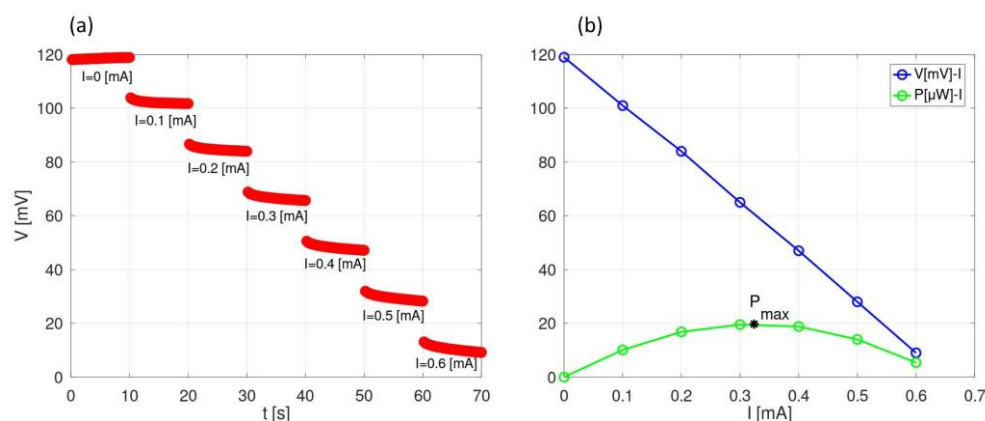


Figure 5. Example of the potentiostat/galvanostat test procedure adopted during the campaign: (a) current steps of 0.1 mA, 10 s long; (a,b) evaluation of power and max power during tests.

3. Results and Discussion

The cell configuration that is representative of a unit for large-scale applications is here represented by a stand-alone system characterized by a large surface-to-volume ratio to optimize the functional thermoelectric surface. To increase the power, it is desirable to have a large cell cross-section area as well as a large electrode surface area. It is well known that thermal convection in thermoelectric cells, apart from increasing mass transfer, also increases heat transfer. Consequently, the large cross-section of the upscaled cell combined with convection would lead to a large thermal exchange, which would reduce the energy efficiency. Therefore, the thermal exchange between the electrodes, which took place between the materials of construction and electrolyte, needs to be minimized. This aspect, together with the need to enhance the mass transport properties of the system, represents the main challenges to be tackled in conceiving the architecture of the up-scaled cell. The design approach here proposed, which consists of a network of parallel, long, thin channels, allows for reduced thermal transport by convection because each channel, being separated by insulating material, cuts down on the formation of large convection eddies while still maintaining a large portion of the electrode surface area available for power generation.

The thermoelectric performance of the upscaled thermocell here proposed was assessed by measuring the output of the cell as a function of the differential temperature between the hot and cold sides (ΔT). In particular, the tests aimed to quantitatively measure the impact of the carbon-based electrodes on the generated power. The OCV and the P_{max} as a function of ΔT are reported in Figure 6, where the power density (P_{max}/S) is calculated considering the active area of the cell, which is defined as the surface of the electrode contained by the O-ring. Figure 6a reveals that the different electrodes do not influence the OCV measured at different temperatures. The dispersion of results at a defined ΔT can be associated with small temperature variations in the system. Furthermore, the OCV characteristic of the 'void' cell does not change when a carbon-base electrode is introduced into the cell. This clearly demonstrates that the additional electrodes do not affect the potential of the thermocell. However, this potential difference represents an equilibrium property of the system; during cell operation, the maximum power output is also limited by various overpotentials within the system. Concerning the ohmic drop, the internal electrical resistance of the cell is not affected significantly by the presence of the carbon-based electrodes due to their reduced thickness and low resistivity. On the other hand, the curves in Figure 6b reveal a trend: the power output clearly depends on the ECSA of the electrodes. In the case of carbon-based electrodes, the greater ECSA increases the number of reaction sites, leading to faster electron transfer kinetics from the redox couple, reducing the charge transfer overpotential, and enhancing the maximum generated power. Specifically, the 39BB electrode, which exhibits its MPL at the interface with the electrolyte, introduces a boost factor of about 3 with respect to its counterparts without

MPL (CC and 39AA). The modification of the 39BB sample with Vulcan XC72 carbon does not entail an improvement in the thermoelectric performance. The Vulcan-based material increased the electric resistivity of the materials but was not able to improve the access of the redox couple inside its porous structure. In fact, the P_{\max} measured with 39BB + V results slightly reduced with respect to the 39BB counterpart, perfectly in line with the relationship between the ECSAs.

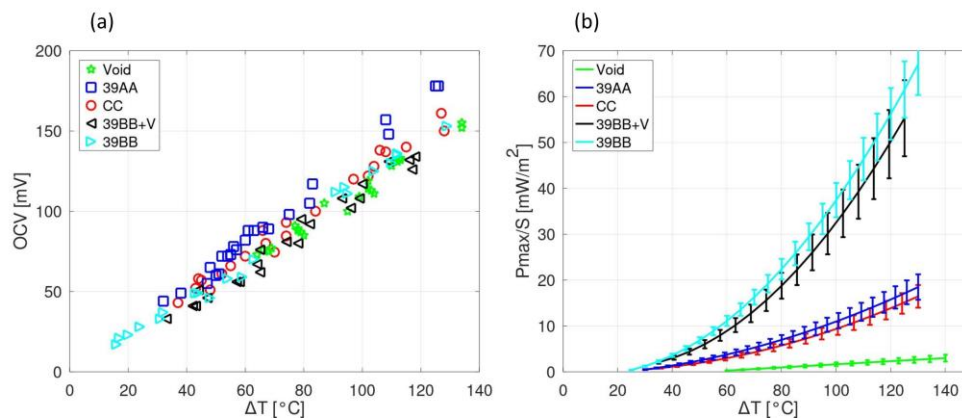


Figure 6. Thermoelectric test results obtained with different electrodes: (a) OCV and (b) P_{\max}/S as a function of the ΔT between the hot and cold sides. The P_{\max}/S curves are obtained by fitting the experimental data using a polynomial regression.

The practical applications of thermocells are limited by the low voltage that can be generated. Although the maximum potential of a single cell will be limited by the Seebeck coefficient and the temperature gradient, the voltage of the future liquid-based TEG can be maximized, as is done in solid semiconductor-based TEG modules, where p-type and n-type semiconductor legs are joined electrically in series and thermally in parallel. There is, however, a general lack of chemically and thermally stable redox species that are soluble in ILs and possess large negative Seebeck coefficients. A possible candidate is $\text{Fe}(\text{CN})_6^{3-/4-}$ (ferri/ferrocyanide). A few groups have reported chemical methods to synthesize organic ferricyanide from potassium-ferricyanide salt [29,30]. The reported Se coefficient in 1-butyl-1-methylpyrrolidinium bis(trifluoromethylsulfonyl)amide (an ionic liquid similar to the one used in this study) is -1.37 mV/K, very close in magnitude to the 1.5 mV/K of the $[\text{Co}(\text{ppy})]^{3+/2+}$ salts examined in this study. Following the steps proposed by Jiang et al., we were able to dissolve $\text{Fe}(\text{CN})_6^{3-}$ in EMIM-TFSI (by replacing the K^+ ions by EMIM+), then electrochemically reduce $\text{Fe}(\text{CN})_6^{3-}$ into $\text{Fe}(\text{CN})_6^{4-}$. However, we could not obtain a stable signal for several days. So further research should be devoted to this field of investigation.

4. Conclusions

This study demonstrates the feasibility of building a thermogalvanic cell at a scale compatible with the construction of a thermoelectric generator. The design challenges and the key performance limitations that need to be addressed for scaling up such a system in real-world applications are discussed. In particular, this paper tackles one of the main hurdles that hampers the performance of thermocells, which is the low rate of electrode reactions. For this purpose, the effective surface area of electrodes was enhanced to considerably increase the number of reaction sites at the electrode/electrolyte interface. Cost-effective carbon-based materials characterized by a large electrochemical surface area were used to evaluate their effect on the generated electrical power. The results of the experimental campaign show a clear dependence of the power output of the cell on the electrochemical surface area of the electrodes in contact with the electrolyte. Consequently, the cells integrating the carbon-based electrodes show thermoelectric performance far better with respect to the Pt electrode-based counterpart.

However, the design and construction of efficient thermogalvanic electric generators for industrial heat recovery require both fundamental studies and further development of the design. In particular, the development of the following solutions is highly required:

- Ionic working fluids are able to resist at very high temperatures ($>300\text{ }^{\circ}\text{C}$), enabling in this way the possibility of exploiting higher temperature gradients.
- Redox couples have high mobility in the working fluid and electrolyte–electrode interface.
- Electrodes with an increased electrochemical surface area could be obtained by tailoring the composition of the microporous layer and selecting active carbon with a pore distribution compatible with the size of the molecules composing the redox couple and the electrolyte.
- The improved system design is able to maximize the temperature gradient between the cold and hot sides of the generator.
- Optimized heat transfer between the heat source and the hot side of the generator (and conversely between the heat sink and the cold).

All these requirements need to be combined with the general stringent constraints for the selection of materials to be used for industrial applications. In particular, the system has to be sustainable from an environmental and economic perspective; the used materials have to be easily recyclable, not toxic to human beings or the environment, and not based on the use of critical raw materials. From this point of view, the identification of a sustainable alternative to the cobalt-based redox couple would represent a further major step due to the concerns related to cobalt environmental toxicity and reduced availability.

Supplementary Materials: The following supporting information can be downloaded at: <https://www.mdpi.com/article/10.3390/en17010001/s1>, Figure S1: Voltammeteries with rotating disk electrode at ambient temperature and 120°C (left). Relationship between current and square root of the angular velocity of the RDE (right). Reference [36] are cited in the supplementary materials.

Author Contributions: Conceptualization, A.B., A.T. (Alessio Tommasi) and G.N.; methodology, A.B., A.T. (Alessio Tommasi) and G.N.; formal analysis, A.B.; investigation, A.B., A.T. (Arianna Tiozzo), R.R. and S.C.Z.; resources, G.N., S.F., S.C.Z. and S.N.; data curation, A.B.; writing—original draft preparation, A.B. and A.T. (Arianna Tiozzo); writing—review and editing, all authors; supervision, S.N. and M.F.S.; funding acquisition, A.T. (Alessio Tommasi), E.L., S.F., S.N. and M.F.S. All authors have read and agreed to the published version of the manuscript.

Funding: This research has received funding from the European Union’s Horizon 2020 research and innovation program under grant number 731976 (MAGENTA project).

Data Availability Statement: This study did not produce any publicly archived datasets or databases. The data presented in this study are available on request from the corresponding author.

Acknowledgments: The authors would like to express their gratitude to Mark Robbins and Dom Cupertino from C-Tech Innovation for their guidance in the device design and to Flavio Parussa from Centro Ricerche Fiat S.C.p.A. for their support in the test setup.

Conflicts of Interest: Authors Andrea Bertinetti and Alessio Tommasi were employed by the company Gemmate Technologies srl, and Sebastien Fantini was employed by the company Solvionic. The remaining authors declare that the research was conducted in the absence of any commercial or financial relationships that could be construed as a potential conflict of interest.

References

1. World Energy Investment 2023—Analysis. Available online: <https://www.iea.org/reports/world-energy-investment-2023> (accessed on 7 August 2023).
2. Bian, Q. Waste Heat: The Dominating Root Cause of Current Global Warming. *Environ. Syst. Res.* **2020**, *9*, 8. [CrossRef]
3. Waste Heat: Innovators Turn to an Overlooked Renewable Resource. Available online: <https://e360.yale.edu/features/waste-heat-innovators-turn-to-an-overlooked-renewable-resource> (accessed on 7 August 2023).
4. Jaziri, N.; Boughamoura, A.; Müller, J.; Mezghani, B.; Tounsi, F.; Ismail, M. A Comprehensive Review of Thermoelectric Generators: Technologies and Common Applications. *Energy Rep.* **2020**, *6*, 264–287. [CrossRef]

5. Loni, R.; Najafi, G.; Bellos, E.; Rajaei, F.; Said, Z.; Mazlan, M. A Review of Industrial Waste Heat Recovery System for Power Generation with Organic Rankine Cycle: Recent Challenges and Future Outlook. *J. Clean. Prod.* **2021**, *287*, 125070. [[CrossRef](#)]
6. Huang, P.; Copertaro, B.; Zhang, X.; Shen, J.; Löfgren, I.; Rönnelid, M.; Fahlen, J.; Andersson, D.; Svanfeldt, M. A Review of Data Centers as Prosumers in District Energy Systems: Renewable Energy Integration and Waste Heat Reuse for District Heating. *Appl. Energy* **2020**, *258*, 114109. [[CrossRef](#)]
7. Zoui, M.A.; Bentouba, S.; Stocholm, J.G.; Bourouis, M. A Review on Thermoelectric Generators: Progress and Applications. *Energies* **2020**, *13*, 3606. [[CrossRef](#)]
8. Yang, J.; Stabler, F.R. Automotive Applications of Thermoelectric Materials. *J. Electron. Mater.* **2009**, *38*, 1245–1251. [[CrossRef](#)]
9. Dan, D.; Zhao, Y.; Wei, M.; Wang, X. Review of Thermal Management Technology for Electric Vehicles. *Energies* **2023**, *16*, 4693. [[CrossRef](#)]
10. Massetti, M.; Jiao, F.; Ferguson, A.J.; Zhao, D.; Wijeratne, K.; Würger, A.; Blackburn, J.L.; Crispin, X.; Fabiano, S. Unconventional Thermoelectric Materials for Energy Harvesting and Sensing Applications. *Chem. Rev.* **2021**, *121*, 12465–12547. [[CrossRef](#)]
11. Quickenden, T.I.; Vernon, C.F. Thermogalvanic Conversion of Heat to Electricity. *Sol. Energy* **1986**, *36*, 63–72. [[CrossRef](#)]
12. Dupont, M.F.; MacFarlane, D.R.; Pringle, J.M. Thermo-Electrochemical Cells for Waste Heat Harvesting—Progress and Perspectives. *Chem. Commun. Camb. Engl.* **2017**, *53*, 6288–6302. [[CrossRef](#)]
13. Salez, T.J.; Nakamae, S.; Perzynski, R.; Mériquet, G.; Cebers, A.; Roger, M. Thermoelectricity and Thermodiffusion in Magnetic Nanofluids: Entropic Analysis. *Entropy* **2018**, *20*, 405. [[CrossRef](#)] [[PubMed](#)]
14. Zhang, L.; Kim, T.; Li, N.; Kang, T.J.; Chen, J.; Pringle, J.M.; Zhang, M.; Kazim, A.H.; Fang, S.; Haines, C.; et al. High Power Density Electrochemical Thermocells for Inexpensively Harvesting Low-Grade Thermal Energy. *Adv. Mater.* **2017**, *29*, 1605652. [[CrossRef](#)]
15. Hupp, J.T.; Weaver, M.J. Solvent, Ligand, and Ionic Charge Effects on Reaction Entropies for Simple Transition-Metal Redox Couples. *Inorg. Chem.* **1984**, *23*, 3639–3644. [[CrossRef](#)]
16. Gonçalves, W.D.G.; Caspers, C.; Dupont, J.; Migowski, P. Ionic Liquids for Thermo-electrochemical Energy Generation. *Curr. Opin. Green Sustain. Chem.* **2020**, *26*, 100404. [[CrossRef](#)]
17. Abraham, T.J.; Macfarlane, D.R.; Baughman, R.H.; Jin, L.; Li, N.; Pringle, J.M. Towards Ionic Liquid-Based Thermo-electrochemical Cells for the Harvesting of Thermal Energy. *Electrochim. Acta* **2013**, *113*, 87–93. [[CrossRef](#)]
18. Hu, R.; Cola, B.A.; Haram, N.; Barisci, J.N.; Lee, S.; Stoughton, S.; Wallace, G.; Too, C.; Thomas, M.; Gestos, A.; et al. Harvesting Waste Thermal Energy Using a Carbon-Nanotube-Based Thermo-Electrochemical Cell. *Nano Lett.* **2010**, *10*, 838–846. [[CrossRef](#)]
19. Inagaki, M.; Konno, H.; Tanaike, O. Carbon Materials for Electrochemical Capacitors. *J. Power Sources* **2010**, *195*, 7880–7903. [[CrossRef](#)]
20. Im, H.; Kim, T.; Song, H.; Choi, J.; Park, J.S.; Ovalle-Robles, R.; Yang, H.D.; Kihm, K.D.; Baughman, R.H.; Lee, H.H.; et al. High-Efficiency Electrochemical Thermal Energy Harvester Using Carbon Nanotube Aerogel Sheet Electrodes. *Nat. Commun.* **2016**, *7*, 10600. [[CrossRef](#)]
21. Artyukhov, D.; Kiselev, N.; Gorshkov, N.; Kovyneva, N.; Ganzha, O.; Vikulova, M.; Gorokhovskiy, A.; Offor, P.; Boychenko, E.; Burmistrov, I. Harvesting Waste Thermal Energy Using a Surface-Modified Carbon Fiber-Based Thermo-Electrochemical Cell. *Sustainability* **2021**, *13*, 1377. [[CrossRef](#)]
22. Burmistrov, I.; Khanna, R.; Gorshkov, N.; Kiselev, N.; Artyukhov, D.; Boychenko, E.; Yudin, A.; Konyukhov, Y.; Kravchenko, M.; Gorokhovskiy, A.; et al. Advances in Thermo-Electrochemical (TEC) Cell Performances for Harvesting Low-Grade Heat Energy: A Review. *Sustainability* **2022**, *14*, 9483. [[CrossRef](#)]
23. Shi, X.-L.; Zou, J.; Chen, Z.-G. Advanced Thermoelectric Design: From Materials and Structures to Devices. *Chem. Rev.* **2020**, *120*, 7399–7515. [[CrossRef](#)] [[PubMed](#)]
24. Wu, T.; Kim, J.; Lim, J.-H.; Kim, M.-S.; Myung, N.V. Comprehensive Review on Thermoelectric Electrodeposits: Enhancing Thermoelectric Performance Through Nanoengineering. *Front. Chem.* **2021**, *9*, 762896. [[CrossRef](#)] [[PubMed](#)]
25. Saleemi, M.; Toprak, M.S.; Li, S.; Johnsson, M.; Muhammed, M. Synthesis, Processing, and Thermoelectric Properties of Bulk Nanostructured Bismuth Telluride (Bi₂Te₃). *J. Mater. Chem.* **2011**, *22*, 725–730. [[CrossRef](#)]
26. Kwon, H.-N.; Jang, S.-J.; Kang, Y.C.; Roh, K.C. The Effect of ILs as Co-Salts in Electrolytes for High Voltage Supercapacitors. *Sci. Rep.* **2019**, *9*, 1180. [[CrossRef](#)] [[PubMed](#)]
27. Ahn, Y.; Kim, B.; Ko, J.; You, D.-J.; Yin, Z.; Kim, H.; Shin, D.; Cho, S.; Yoo, J.; Kim, Y.S. All Solid State Flexible Supercapacitors Operating at 4 V with a Cross-Linked Polymer-Ionic Liquid Electrolyte. *J. Mater. Chem. A* **2016**, *4*, 4386–4391. [[CrossRef](#)]
28. dos Santos Junior, G.A.; Fortunato, V.D.S.; Bastos, G.A.A.; Silva, G.G.; Ortega, P.F.R.; Lavall, R.L. High-Performance Lithium-Ion Hybrid Supercapacitors Based on Lithium Salt/Imidazolium Ionic Liquid Electrolytes and Ni-Doped LiMn₂O₄ Cathode Materials. *ACS Appl. Energy Mater.* **2020**, *3*, 9028–9039. [[CrossRef](#)]
29. You, D.-J.; Yin, Z.; Ahn, Y.; Lee, S.-H.; Yoo, J.; Kim, Y.S. Redox-Active Ionic Liquid Electrolyte with Multi Energy Storage Mechanism for High Energy Density Supercapacitor. *RSC Adv.* **2017**, *7*, 55702–55708. [[CrossRef](#)]
30. Laux, E.; Jeandupeux, L.; Uhl, S.; Keppner, H.; Pérez López, P.; Sanglard, P.; Vanoli, E.; Marti, R. Novel Ionic Liquids for Thermoelectric Generator Devices. *Mater. Today Proc.* **2019**, *8*, 672–679. [[CrossRef](#)]
31. Al-Masri, D.; Dupont, M.; Yunis, R.; MacFarlane, D.R.; Pringle, J.M. The Electrochemistry and Performance of Cobalt-Based Redox Couples for Thermo-electrochemical Cells. *Electrochim. Acta* **2018**, *269*, 714–723. [[CrossRef](#)]

32. Bozack, M.J.; Zhou, Y.; Worley, S.D. Structural Modifications in the Amino Acid Lysine Induced by Soft X-ray Irradiation. *J. Chem. Phys.* **1994**, *100*, 8392–8398. [[CrossRef](#)]
33. Yu, X.-R.; Liu, F.; Wang, Z.-Y.; Chen, Y. Auger Parameters for Sulfur-Containing Compounds Using a Mixed Aluminum-Silver Excitation Source. *J. Electron Spectrosc. Relat. Phenom.* **1990**, *50*, 159–166. [[CrossRef](#)]
34. Hao, L.H.; Hieu, D.T.T.; Danh, T.T.; Long, T.H.; Phuong, H.T.; Luan, L.Q.; Man, T.V.; Tuyen, L.A.; Ngoc, P.K.; Tap, T.D. Surface Features of Polymer Electrolyte Membranes for Fuel Cell Applications: An Approach Using S2p XPS Analysis. *VNUHCM J. Sci. Technol. Dev.* **2021**, *24*, 2100–2109. [[CrossRef](#)]
35. Worley, C.M.; Vannet, M.D.; Ball, G.L.; Moddeman, W.E. Surface Chemistry of a Microcoated Energetic Material, Pentaerythritol tetranitrate (PETN). *Surf. Interface Anal.* **1987**, *10*, 273–279. [[CrossRef](#)]
36. Bard, A.J.; Faulkner, L.R. *Electrochemical Methods: Fundamentals and Applications*; Wiley: New York, NY, USA, 2001; ISBN 978-0-471-04372-0.

Disclaimer/Publisher's Note: The statements, opinions and data contained in all publications are solely those of the individual author(s) and contributor(s) and not of MDPI and/or the editor(s). MDPI and/or the editor(s) disclaim responsibility for any injury to people or property resulting from any ideas, methods, instructions or products referred to in the content.